Journal of Physical Chemistry & Biophysics
ISSN: 2161-0398
Combs et al., J Phys Chem Biophys 2016, 6:1
DOI: 10.4172/2161-0398.1000202
Review Article
Open Access

Surface FTIR Techniques to Analyze the Conformation of Proteins/Peptides in H_2O Environment

Joseph D Combs, Cuauhtemoc U Gonzalez and Chengshan Wang*

Chemistry Department, Middle Tennessee State University, Murfreesboro, TN 37132, United States of America

Abstract

Proteins/peptides, which are involved in various biochemical processes in biological systems, contain infrared (IR) active vibrations. Among all the IR absorption bands of proteins/peptides, the amide I band arises mainly from the stretching vibration of the carbonyls (C=O) in backbone amide bonds and is sensitive to the conformations (such as α–helix, β–sheet, unstructured conformation, and so on) in a protein/peptide. Therefore, the amide I band has been used to monitor the biophysical/biochemical behavior of proteins/peptides in biological samples (e.g., living cells or tissues). However, obtaining reproducible IR spectra of proteins/peptides in H_2O solution was challenging by direct transmission measurement using a liquid cell with milli-meter level path length, due to the intensive IR absorption of H_2O around 1620 cm^{-1} which overlaps the amide I band. Thus, lots of the IR spectra of proteins/peptides were accomplished in D_2O, which has IR absorption around 1200 cm^{-1}. Since D_2O may not be a favorable solvent for biological samples, the position of the amide I band of various conformations was needed as a reference for biological samples. Consequently, various surface FTIR techniques (such as Infrared Reflection-Absorption Spectroscopy or IRRAS, and Attenuated Total Reflection or ATR) have been developed to obtain the IR spectra of proteins/peptides in H_2O environment and have been reviewed here.

Keywords: Amide I band; IRRAS; PM-IRRAS; ATR; Langmuir monolayer; ^{13}C labels

Introduction

Background of peptides/proteins

Proteins are biological macro-molecules which are involved in various biochemical processes (e.g., oxidative phosphorylation [1,2], DNA replication [3,4], response to stimuli [5,6] and so on [7,8]). All the proteins found in biological systems comprise amino acids as shown in Figure 1 [9-11]. An α-carbon is at the center of an amino acid and is covalently linked to an amine group, a carboxylic group, hydrogen atom, and a residue group (i.e., the R group). Amino acids are distinguished according to the structure of the R group as shown in Table 1. When covalently linking amino acids by amide bonds (O=C-NH in which the carbonyl group is from one amino acid and NH is from the adjacent amino acid as shown in Figure 1), the polypeptide chain of peptides (shorter polypeptide chains) or proteins (longer chains) is formed.

The sequence of the amino acids in the polypeptide chain of peptides/proteins is the primary structure. The two termini of a polypeptide chain are termed as the N-terminus (it has a free amine group) and the C-terminus (it has a free carboxylic acid group). Because of the large number of amino acids in a protein, an abbreviation is used for every amino acid as shown in Table 1 to describe the protein sequence, which is usually written from N-terminus to C-terminus. For example, the sequence of a model peptide is HAAKAAAAKAAAAKAAY, which will be discussed in detail later in this review. Abbreviations with three letters are also used when discussing specific positions. The N-terminal residue (or the first residue) of the model peptide above is histidine, which can be referred to as either His1 or H1.

The secondary structure of a protein is the specific geometric shape caused by the intra and inter-molecular hydrogen bonding of amide groups. Typical secondary structures (also called conformations) are α–helix, β–sheets, and random coil [12-14]. Random coil structure is also called unstructured conformation, in which the polypeptide chain is well dissolved in the aqueous solution and moves freely in the aqueous environment. As a very common secondary structure, α–helix is characterized by the intra molecular hydrogen bonds between the amine group of one amino acid and the carbonyl group of another amino acid located 3~4 residues away along the polypeptide chain [13]. These hydrogen bonds are roughly parallel to the helical axis. The α-helix is usually right handed and contains approximately 3.6 amino acid residues per turn. The structural units of β–sheets are strands, which are fully extended structures characterized by multiple polypeptide strands arranged side-by-side [12]. Side chains are present above and below the plane of the polypeptide chain. Inter-strand hydrogen bonds are formed between the carbonyl oxygen of one chain and the amide hydrogen of the other chain.

Techniques to determine a protein's/peptide's structure

As mentioned above, proteins perform a variety of functions in biological systems, and their activity is influenced by the structure. Thus, techniques have been developed to determine the structure of proteins/peptides. X-ray crystallography is a widely used technique to address proteins structure by the diffraction of the X-ray from a single crystal of target proteins. However, lots of proteins cannot form a single crystal. Not requiring proteins to form single crystal, nuclear magnetic resonance (NMR) is another powerful technique to elucidate the structure of proteins. To obtain a high resolution of the structure, multidimensional NMR measurement of proteins is usually time consuming. Therefore, it is challenging for NMR to "snapshot" protein

***Corresponding author:** Chengshan Wang, Chemistry Department, Middle Tennessee State University, Murfreesboro, TN 37132, United States of America, Tel: 6156929167; E-mail: chengshan.wang@mtsu.edu

Received January 18, 2016; **Accepted** February 05, 2016; **Published** February 09, 2016

Citation: Combs JD, Gonzalez CU, Wang C (2016) Surface FTIR Techniques to Analyze the Conformation of Proteins/Peptides in H_2O Environment. J Phys Chem Biophys 6: 202. doi:10.4172/2161-0398.1000202

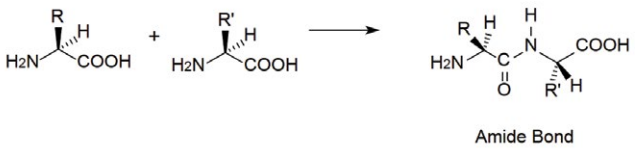

Figure 1: Structure of an amino acid and the formation of the amide bond.

Amino acid	Abbreviations		Structure of R group shown in Figure 1
Alanine	Ala	A	$-CH_3$
Arginine	Arg	R	$-(CH_2)_3-NH-C(NH_2)=NH$
Asparagine	Asn	N	$-CH_2-CO-NH_2$
Aspartic acid	Asp	D	$-CH_2-COOH$
Cysteine	Cys	C	$-CH_2-SH$
Glutamine	Gln	Q	$-(CH_2)_2-CO-NH_2$
Glutamic Acid	Glu	E	$-(CH_2)_2-COOH$
Glycine	Gly	G	$-H$
Histidine	His	H	$-CH_2C_3H_3N_2$
Isoleucine	Ile	I	$-CH(CH_3)-CH_2-CH_3$
Leucine	Leu	L	$-CH_2-CH-(CH_3)_2$
Lysine	Lys	K	$-(CH_2)_4NH_2$
Methionine	Met	M	$-(CH_2)_2-S-CH_3$
Phenylalanine	Phe	F	$-CH_2-C_6H_5$
Proline	Pro	P	$-CH(CH_2)_3NH$
Serine	Ser	S	$-CH_2-OH$
Threonine	Thr	T	$-CH(OH)-CH_3$
Tryptophan	Trp	W	$-CH_2-C_8H_6N$
Tyrosine	Tyr	Y	$-CH_2-C_6H_5-OH$
Valine	Val	V	$-CH-(CH_3)_2$

Table 1: Structure of R groups of amino acids.

species with short life-times. In addition, repeating sequences in proteins will cause the overlap of NMR signals and result in difficulties in the analysis of the data. In contrast, Infrared (IR) techniques which have a quick response and are able to provide high resolution results have been developed to address the structure of proteins.

Fourier Transform IR (FTIR) spectroscopy

FTIR spectroscopy detects the vibrations in a molecule. As shown in Figure 1, proteins/peptides contain groups with IR active vibrations such as the amide group (i.e., O=C-NH), αC-H, and residue groups of amino acids. These groups result in several intensive bands in the FTIR spectra. For example, the amide A band around 3300 cm^{-1} is from the N-H stretching vibration in the amide group. The amide I band (mainly from the stretching mode of C=O in the amide group) and amide II bands (from the bending mode vibration of N-H in amide group) are in the range of 1600-1700 cm^{-1} and 1500-1560 cm^{-1}, respectively. Among all the amide bands, the position of the amide I band is most sensitive to the conformation (i.e., the secondary structures) change of proteins/peptides and has been widely used to evaluate the fraction of various secondary structures in a protein/peptide.

Heavy water (D_2O) is more widely used to obtain the FTIR spectra of proteins/peptides

Lots of FTIR spectra of proteins/peptides were obtained in D_2O [15-20], not H_2O, because the intensive IR absorption of H_2O between 1500 to 1800 cm^{-1} overlaps the position of the amide I band [21,22]. Thus, the amide I band in the FTIR spectra of proteins/peptides can be clearly detected in D_2O with the background IR absorption around 1200 cm^{-1} [21,22]. However, there are reasons to obtain the FTIR spectra of proteins/peptides in H_2O rather than D_2O. For example, *in vivo* proteins reside in an H_2O environment and D_2O is not favorable to biological systems [23,24]. For the analysis of the FTIR results of biological samples (such as living cells and tissue samples), the amide I band in H_2O is needed as a reference [23,25,26]. Thus, efforts to obtain the FTIR spectroscopy of proteins/peptides in the absence of D_2O have been tried by various methods, which are reviewed here in the order of the time when they were invented.

Techniques to Obtain FTIR Spectroscopy of Peptides/Proteins in H_2O Environment

Sample cells of CaF2 with the path length of 0.01 mm

CaF_2 slides are widely used to construct sample containers for FTIR spectroscopy due to its very low background absorption [21,27,28]. Thus, CaF_2 windows have been used first to build up homemade cells with a minimum path length of 0.01 mm (i.e., 10 μm) [21]. By this method, the amide I band was measured in both H_2O and D_2O environments and the amide I band of a certain protein was found to be 5-15 cm^{-1} higher in H_2O than that in D_2O, because of H/D exchange [21]. Notice that the actual path length of this cell might be affected by the surface roughness of the CaF_2 windows. Therefore, it may be challenging to use this kind of cell to obtain reproducible FTIR results of proteins/peptides in H_2O.

Reduce the H_2O absorption by organic solvent

Increasing the path length of the above-mentioned CaF_2 cell to 0.025 mm has been shown to improve reproducibility [28]. However, the H_2O background absorption was too strong through a path length of 0.025 mm and made the detection of the amide I band difficult. To decrease the H_2O absorption under this circumstance, organic solvents (such as dioxane) soluble in H_2O have been used to dilute H_2O and consequently decrease the H_2O background absorption [28]. However, the amide bands of proteins/peptides shifted and the quantitative analysis of the conformation of a protein was challenging, because the organic solvent may change the hydration of the amide groups [28].

FTIR spectroscopy of proteins in Langmuir-Blodgett films

Proteins have been also spread at the air-water interface and then transferred onto solid substrates to form a Langmuir-Blodgett (LB) film, which can be analyzed by FTIR spectroscopy in the absence of D_2O. High quality and reproducible results of the FTIR spectroscopy of proteins/peptides can be obtained [29-32]. However, small amount of the remaining H_2O which is strongly absorbed by protein molecules in the LB film may be evaporated. To maintain the protein molecules in an H_2O environment, IR Reflection-Absorption Spectroscopy (IRRAS) which can measure the FTIR spectroscopy of proteins at the air-water interface has been developed.

IRRAS studies of proteins at the air-water interface

Amphiphilic molecules such as stearic acid, which contains both a hydrophilic head group and a hydrophobic alkyl chain, can form a Langmuir monolayer (i.e., one single layer of molecules) at the air-water interface. The technique of IRRAS for the Langmuir monolayer was developed in 1985 [33]. Subsequently, some proteins were shown to be also able to form a Lanmguir monolayer and IRRAS has been consequently used to analyze protein samples in the Langmuir monolayer [14,34-38], which covers the surface of H_2O. IRRAS can not only detect the FTIR signal of proteins, but also valuate the orientation of the proteins sample in the Langmuir monolayer due to the selection rules as discussed below [14,34-36,38].

Selection rules of IRRAS: There are two variables enabling IRRAS to evaluate the orientation of vibrations of the molecules in Langmuir monolayer. One variable is the polarization of the incident IR beam and the other is the incident angle, which is the angle between the incident IR beam and the normal of the air-water interface [38,39]. As shown in Figure 2, the incident IR beam and the normal of the air-water interface compose the incident plane. If the electric field of the incident IR beam is polarized in the incident plane, the IR is p-polarized [38,39]. The IR is s-polarized when the electrical field is perpendicular to the incident plane [38,39]. The peak intensity of a certain vibration depends on the orientation of the vibration, the polarization, and the incident angle. Because both the polarization and the incident angle can be monitored accurately during the measurement of IRRAS, the orientation of a certain vibration can be evaluated in the following.

The s-polarized IRRAS can only detect the vibrations parallel to the air-water interface and the peak intensity of a certain vibration in the s-polarized IRRAS decreases with the increasing incident angle. Because almost no vibration in reality is absolutely perpendicular to the air-water interface, s-polarized IRRAS can detect almost all the IR active vibrations in the Langmuir monolayer. On the other hand, the p-polarized IRRAS is widely used to determine the orientation of vibrations in the Langmuir monolayer. For vibrations parallel to the interface, the peaks are initially negative and the peak intensity increases with an increase of the incident angle until the Brewster angle (e.g., 54.2° for the IR light at 2850 cm^{-1} reflected from the surface of water) is reached [38,39]. Above the Brewster angle, there is an inversion of the peaks to positive values and the intensity decreases with a further increase of the incident angle. Regarding a vibration perpendicular to the interface, the opposite should be observed for the sign (positive or negative) of the peak: The peak is positive when the incident angle is below Brewster angle and, becomes negative after the incident angle is above Brewster angle [38,39]. For a tilted vibration, the peak intensity in the p-polarized IRRAS is weak and sometimes the peak disappears.

IRRAS of example protein: The s- and p-polarized IRRAS results of the Langmuir monolayer of oganophosphorus acid anhydrolase (OPAA) are shown in Figure 3a and 3b, respectively [35]. OPAA contains most of the typical conformations (i.e., unstructured conformation, α-helix, β-sheet, turns and so on) as discussed above. The amide I band of turns, α-helix, unstructured conformation, and β-sheet has been reported to be at 1672, 1650, 1640, and 1630 cm^{-1}, respectively. In Figure 3a, all of the above-mentioned peaks have been detected. The intensive peak at 1650 cm^{-1} in Figure 3a indicates the high fraction of α-helix in OPAA whereas the low peak intensity at 1630 cm^{-1} indicates the low fraction of β-sheet. However, the peak intensity of 1630 cm^{-1} was strong in the p-polarized IRRAS as shown in Figure 3b. Because the amide I band is mainly from the vibration of carbonyls (C=O) in the amide bond, the carbonyls in amide bond in the β-sheet conformation of OPAA in the Langmuir monolayer should be parallel to the air-water interface. Interestingly, the amide I band of unstructured conformation at 1640 cm^{-1} was not detected in p-polarized IRRAS. This result is reasonable because the carbonyls in unstructured conformation should be randomly distributed and this orientation is not preferred by p-polarized IRRAS, as discussed in the above section about the selection rules of IRRAS [35]. Similarly, some other proteins with high fraction of α-helix have been analyzed by IRRAS and important information about the change of both the conformation and orientation of the proteins has been addressed [35].

IRRAS of proteins with other conformations than α-helix: The prerequisite of the IRRAS measurement of protein samples at the air-water interface is that the protein can form a Langmuir monolayer. Among the various conformations, α-helix has been shown to help proteins to form a Langmuir monolayer [40]. It is difficult for proteins with a high fraction of unstructured conformation to form the monolayer. This may be because of the extensive hydration of unstructured proteins/peptides with the bulk H_2O molecules. To facilitate the measurements of the IRRAS of proteins in other conformations than α-helix, the Langmuir monolayer of phospholipids has been used to adsorb proteins onto the interface [41]. For example, β-amyloid (Aβ) can form various types of aggregates, which are in β-sheet conformation and have been shown to be responsible for

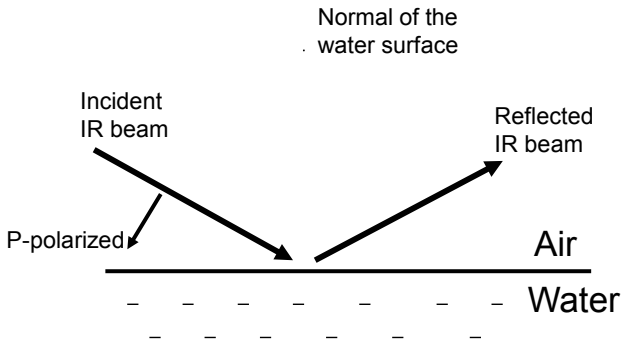

Figure 2: The illustration of IRRAS. The electric field direction of the p-polarized IR beam is in the incident plane and perpendicular to the direction of the IR beam. The electric field of the s-polarized IR beam is perpendicular to the incident plane and is not shown here.

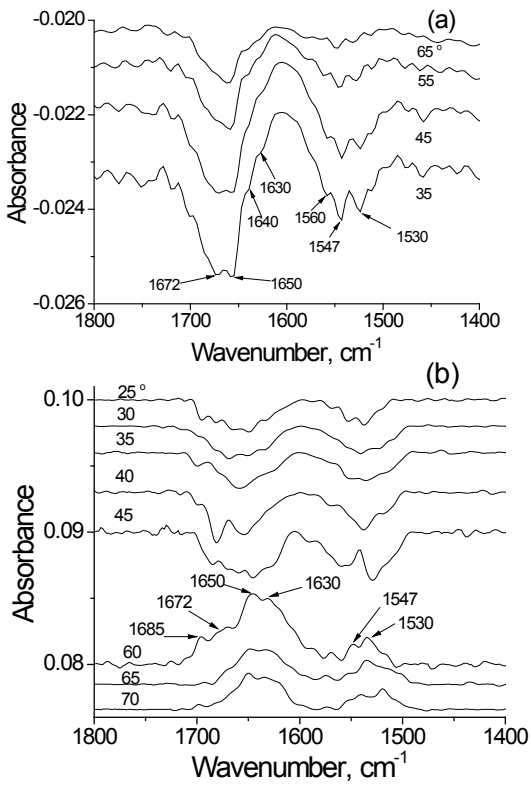

Figure 3: (a) S-polarized and (b) p-polarized IRRAS spectra of the OPAA Langmuir monolayer at surface pressure of 15 $mN \cdot m^{-1}$ with different incident angles. Adapted from Reference [35], copy right 2008 American Chemical Society.

Alzheimer's disease [42,43]. The aggregates can adsorb to the Langmuir monolayer of phospholipids and the p-polarzied IRRAS results showed that the carbonyls in the amide bond in the β-sheet are parallel to the interface [41].

Covalently linking short peptides to lipid molecules: It is still difficult for short peptides to go up to the air-water interface even in the presence of the Langmuir monolayer of phospholipids. To examine the IRRAS of short peptides, a covalently linked hydrophobic alkyl chain may be necessary to keep short peptides at the interface [32]. A short peptide with sequence of FWSHE has been used to mimic the structure of acetylcholinesterase [37], which contains an active site (comprising amino acid S, H, and E) and an aromatic gauge (comprising residues aromatic groups such as F and W) [44]. Due to its good solubility in H_2O, FWSHE was linked to a stearoyl chain to form a peptidolipid to be analyzed by IRRAS as shown in Figure 4 [38]. As shown in Figure 4a, the s-polarized IRRAS detected all the vibrations in the peptidolipid. For example, the alkyl chains signal was detected at 2854 and 2923 cm^{-1}. The amide I and amide II band was detected in the range of 1630-1660 and 1500-1557 cm^{-1}, respectively. In addition, the vibration from the aromatic residue groups of F and W was also detected at 1580 cm^{-1}. However, the peak from aromatic groups disappeared in the p-polarized IRRAS (*c.f.*, Figure 4b) and the peak intensity of the alkyl chains was also weak. Thus, a tilted orientation of the aromatic rings and the alkyl chains was indicated. Interestingly, a specific interaction of this peptidolipid with paraoxon (a pesticide that can deactivate acetylcholinesterase) has been detected but the mechanism of the interaction was not known. Thus, IRRAS was utilized to address the interaction as discussed below [38].

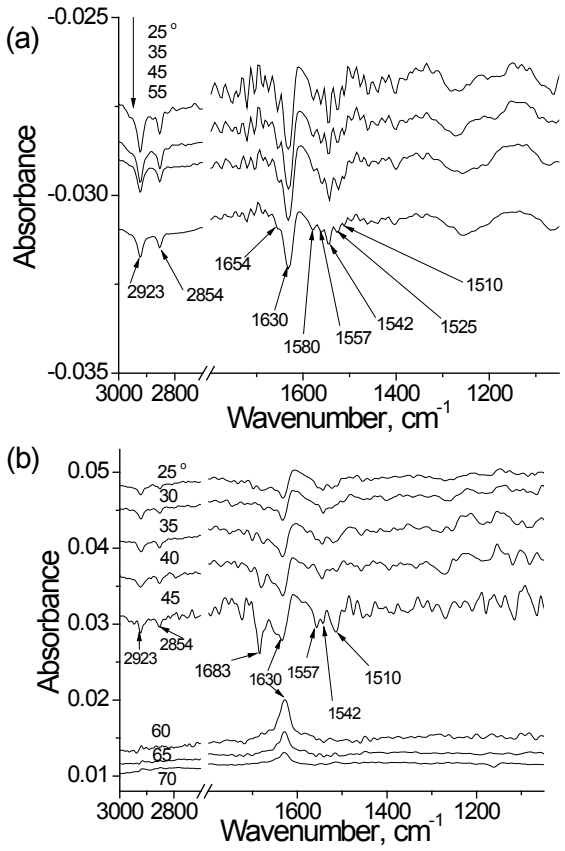

Figure 4: (a) S-polarized and (b) p-polarized IRRAS of the peptidolipid Langmuir monolayer on pure water at 20 $mN \cdot m^{-1}$ against different incident angles. Adapted from Reference [38], copy right 2007 American Chemical Society.

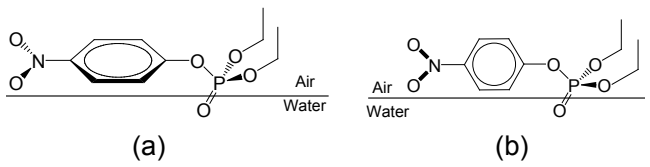

Figure 5: Free rotation of benzene ring of paraoxon when accumulated at the air-water interface. Adapted from Reference [38], copy right 2007 American Chemical Society.

Although not being able to form a stable Langmuir monolayer, paraoxon can still accumulate at the air-water interface. IRRAS results showed that the axis of the nitro-benzene is parallel to the air-water interface as shown in Figure 5a and the benzene ring can rotate freely (*c.f.*, Figure 5b). The IRRAS results of paraoxon H_2O solution was shown below in Figure 6 [38].

Paraoxon has several IR active vibrations and two vibrations are very important, namely the asymmetric and symmetric vibrations of nitro group at 1526 and 1348 cm^{-1}, respectively. Both of the peaks are intensive in the IR spectrum of the bulky paraoxon. However, the peak of the asymmetric vibration at 1526 cm^{-1} was weak in the s-polarized IRRAS (Figure 6a) of paraoxon and even disappeared in the p-polarized IRRAS as shown in Figure 6b. On the contrary, the peak of the symmetric vibration at 1348 cm^{-1} was very strong in both the s- and the p-polarized IRRAS. The only explanation is that the axis of the nitro-benzene of paraoxon is parallel to the air-water interface as shown in Figure 5a. This orientation makes the peak of the symmetric vibration intensive in both s- and p-polarized IRRAS. On the other hand, the benzene ring may rotate freely around the axis and this rotation makes the average orientation of the asymmetric vibration randomly distributed. As a consequence, the peak intensity at 1526 cm^{-1} is weak in Figure 6. Then, what is the mechanism of the specific interaction between paraoxon and the peptidolipid? IRRAS results of the peptidolipid in the presence of paraoxon are shown in Figure 7 [38].

In the presence of the peptidolipid, both the peak of asymmetric vibration at 1526 cm^{-1} and that of symmetric one at 1348 cm^{-1} were weak in both the s-polarized (Figure 7a) and the p-polarized IRRAS results (Figure 7b). It is normal that the asymmetric vibration disappears in the s-polarized IRRAS because of its overlapping with the amide II band of the peptidolipid (Figure 7a). However, there is no overlapping between the peak of symmetric vibration of paraoxon at 1348 cm^{-1} with the peptidolipid. The peak at 1348 cm^{-1} was much weaker in Figure 7a than that in Figure 6a, both of which were s-polarized IRRAS. In addition, the peak at 1348 cm^{-1} disappeared completely in the p-polarized IRRAS (Figure 7b). Thus, Figure 7b indicates a tilted orientation of the axis of the nitro-benzene ring in paraoxon in the presence of the peptidolipid. Interestingly, the peak of the aromatic group in the peptidolipid at 1580 cm^{-1} also disappeared in Figure 7b. Thus, the nitro-benzene ring of paraoxon may be parallel to the aromatic group in the peptidolipid and a π-π interaction between paraoxon and the peptidolipid was reasonable, especially considering the fact that the fluorescence of W in the peptidolipid was quenched in the presence of paraoxon [38].

Polarization modulated IRRAS (PM-IRRAS)

The peak of water vapor is also intensive in the range of 1400-1800 cm^{-1}, which overlaps with the amide I and amide II bands of proteins/

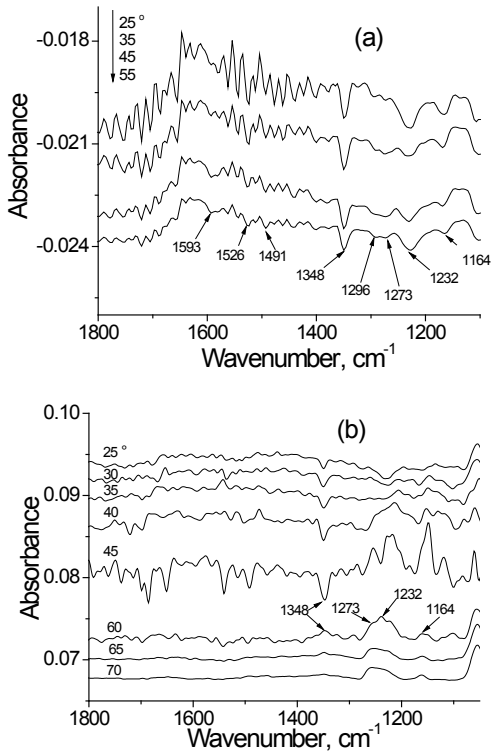

Figure 6: S-polarized (a) and p-polarized (b) IRRAS of paraoxon subphase at the concentration of 1.5×10^{-3} M. Adapted from Reference [38], copy right 2007 American Chemical Society.

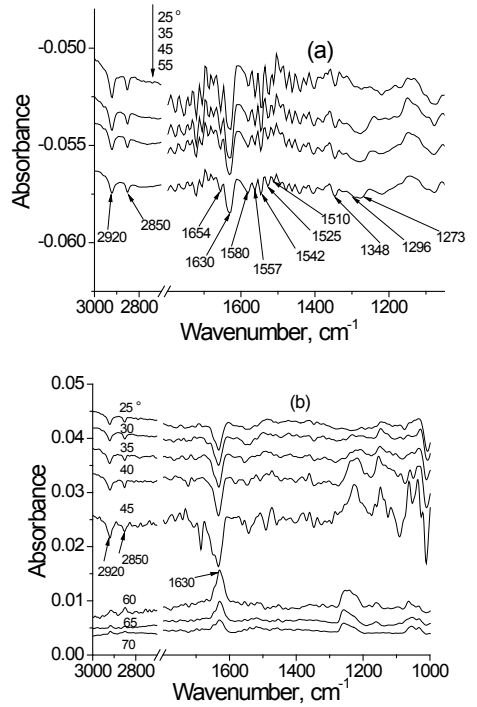

Figure 7: (a) s-Polarized and (b) p-polarized IRRAS of the peptidolipid Langmuir monolayer on paraoxon subphase at a concentration of 1.5×10^{-3} M at 20 mN·m^{-1} against different incident angles. Adapted from Reference [38], copy right 2007 American Chemical Society.

peptides. The water vapor background IR absorption can be removed by either vacuum, pure N_2 purging, or dry air purging. However, the above-mentioned methods may not work well for IRRAS because of the water subphase. During the measurement of IRRAS of a Langmuir monolayer at the air-water interface, a vacuum cannot be applied and pure N_2 or dry air purging will not remove the water vapor from the continuous H_2O evaporation of the water subphase. Although methods of delicate humidity control have been reported recently [38,39], a method able to automatically remove the water vapor IR absorption was welcomed and PM-IRRAS was developed as a consequence [34,45,46].

PM-IRRAS is similar to IRRAS and the difference between them stems from the polarization, which is switched between s- and p-polarization at a set frequency in PM-IRRAS. The PM-IRRAS signal is derived from results of p-polarization minus those of the s-polarization. Then, this subtraction was divided by the sum of the two polarized results. Thus, any isotropic vibration (i.e., the vibration with randomly distributed orientation) will disappear. The vibrations of water vapor disappear in the PM-IRRAS results due to its isotropic orientation in the air [34,45,46]. When the incident angle is above the Brewster angle, the selection rule of PM-IRRAS is very similar to the p-polarized IRRAS: the peak will be positive if the vibration is parallel to the air-water interface. For example, the PM-IRRAS of OPAA is shown in Figure 8. The positive amide I band in Figure 8 indicates that the carbonyls in various conformations are parallel to the air-water interface [35].

Attenuated total reflection (ATR) technique

Although covalently linking short peptides to alkyl chains helps them to migrate to the air-water interface for IRRAS measurements, the biophysical and biochemical behavior of the short peptides or proteins may be affected substantially by alkyl chains. To measure the FTIR spectra of peptides/proteins without any external groups in H_2O, ATR technique was developed. By monitoring the path length accurately in micro-meter level, ATR technique can measure the proteins/peptides IR spectroscopy in H_2O environment with very good reproducibility [47,48] A crystal with high refractive index is usually used for ATR technique, which is illustrated in Figure 9 [49]. When the IR beam is introduced onto the interface with an incident angle θ, both the reflection and refraction occurs. The reflected angle is also θ and the refractive angle is Φ. The relationship between θ and Φ is given by the equation $n_1 \sin\theta = n_2 \sin\Phi$, where n_1 is the refractive index of the incident material (i.e., the crystal) and n_2 is that of the refractive material. In the ATR technique for the H_2O solution samples of proteins/peptides, n_1 (the refractive index of the crystal) is usually bigger than n_2 (which is the refractive index of H_2O) and consequently, θ is smaller than Φ. When the value of sinΦ reaches 1 (i.e., Φ reaches 90°), all the incident IR beam is reflected and no refraction occurs. This phenomenon is called total reflection. However, the incident IR beam still goes into the H_2O phase about 0.1λ (λ is the wavelength of the incident IR) during each total reflection [49]. Thus, the IR beam will be absorbed by the H_2O solution containing the proteins/peptides sample and becomes weaker during each total reflection. Therefore, this technique is termed as "attenuated total reflection". By varying the dimension of the crystal and the incident angle, the number of total reflections can be manipulated and the path length of the IR beam in the H_2O sample can be controlled accurately in micro-meter level [47,48]. Thus, ATR can measure the FTIR spectra of all types of proteins/peptides in H_2O environment and has been widely used [50,51]. Since being reviewed by other papers [50,51], the ATR FTIR results of proteins/peptides are

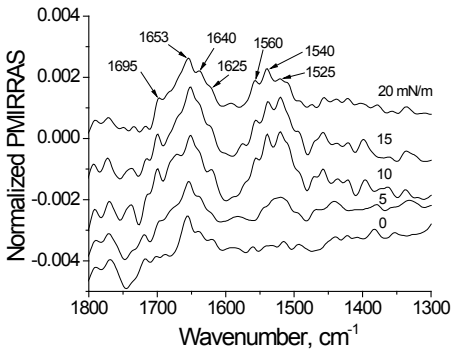

Figure 8: PM-IRRAS spectra of the OPAA Langmuir monolayer with an incident angle at 70°. Adapted from Reference [35], copy right 2008 American Chemical Society.

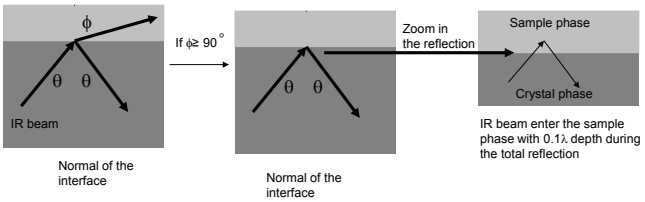

Figure 9: The illustration of the ATR technique.

not covered in this paper.

ATR FTIR spectroscopy of peptides with ^{13}C labeled carbonyls

It has been shown that the fraction of conformations in a certain protein/peptide can be calculated by deconvolulting the amide I band. However, only the overall fraction of various conformations can be evaluated and no information can be provided about the conformation of the local (or specific) residues. Thus, ^{13}C labels have been introduced into the carbonyl groups in the backbone amide bond of peptides and a new band (i.e., the ^{13}C amide I band) was generated as a consequence [17,18]. The ^{13}C amide I band which is in the range from 1585-1610 cm^{-1} has been shown to depend on the conformation of the ^{13}C labeled residue (or amino acid) in D_2O. For example, the ^{13}C amide I' band (i.e., the amide I band in D_2O) of α-helix has been shown to be around 1596 cm^{-1} and that of anti-parallel β-sheet was at either 1590 cm^{-1} or 1600 cm^{-1} [19,20]. Interestingly, the ^{13}C amide I band was not detected when the ^{13}C labeled residue was in unstructured conformation [20]. Because every residue can be ^{13}C labeled as desired during the synthesis of the peptide, the conformation of every residue can be screened by the ^{13}C amide I' band.

To verify that ^{13}C-edited FTIR spectroscopy can be also used in H_2O environment, ^{13}C labeled carbonyls were introduced into the model peptide with sequence HAAKAAAAKAAAAKAAY (Pep17) [52]. At pH 5.0, Pep17 is unstructured conformation if its N-terminus is not covalently linked to an acetyl group. At pH 12.5, most of the residues of Pep17 transform to α-helix but several residues are still in unstructured conformation [52]. To address the residues still in unstructured conformation at pH 12.5, the FTIR spectra of Pep17 with ^{13}C labels at different specific residues in H_2O were studied by ATR and the results are shown in Figure 10 [52]. At pH 5, no ^{13}C amide I band was detected for both unlabeled and ^{13}C labeled Pep17 as shown in Figure 10a. This means that the ^{13}C amide I band of unstructured conformation cannot be detected in H_2O, either. At pH 12.5, the ^{13}C amide I band at 1602 cm^{-1} appeared in the FTIR spectra for the Pep17 with ^{13}C labels at N-terminal residues or the residues in the middle of Pep17. However, the ^{13}C amide I band was absent in the FTIR spectrum of Pep17 with ^{13}C labels at C-terminal residues (cf. Figure 10b). Therefore, the C-terminal residues are still in unstructured conformation even at pH 12.5 [52].

The Amide I Band Used as a Reference for Biological Samples and Future Perspectives

By the above-mentioned surface FTIR methods, the amide I band of various conformations has been determined in an H_2O environment [13,21,34,53-55]. For example, the amide I band of α-helix is around 1650 cm^{-1} and that of unstructured conformation is around 1640 cm^{-1}. The amide I band of β-sheet (at ~1630 cm^{-1} as well as ~1685 cm^{-1}) and that of other conformations such as β-turns have been also determined [13,21,34,53-55]. The position of the amide I band in H_2O has been widely used as a reference to address the conformation of proteins in tissues and living cells [23,25,26], both of which are in H_2O environment. It is probable that ^{13}C labeled peptides will be induced into living cells to obtain information about the behavior of specific region of the ^{13}C labeled peptide/protein in the living cells. Notice that the ^{13}C amide I' band of various conformations in D_2O has been determined systematically [17-20]. However, just like what has been done for the regular amide I band in H_2O, the ^{13}C amide I band in H_2O will be welcomed as a reference to track specific ^{13}C labeled peptide/protein in the samples of tissues and living cells. Compared with regular amide I band of various conformations in H_2O environment, work still remains to be done for the ^{13}C amide I band in H_2O. To the best of our knowledge, only the ^{13}C amide I band of α-helix and unstructured conformation in H_2O has been studied as mentioned above. Therefore, the ^{13}C amide I band of β-sheet and other remaining conformations still needs to be studied,

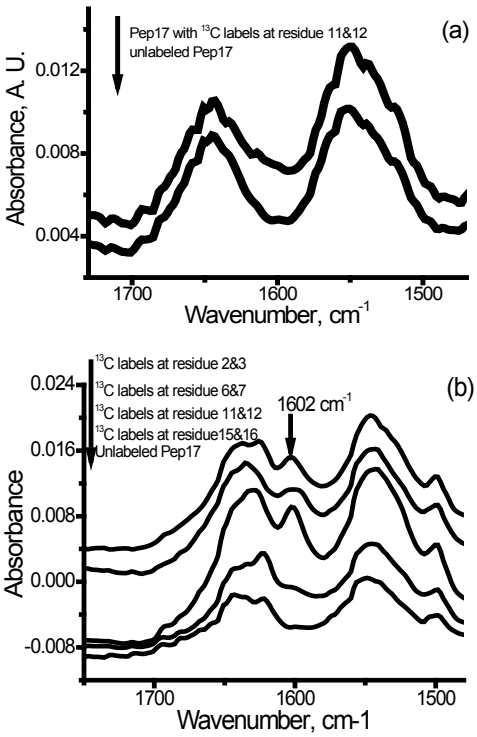

Figure 10: ATR FTIR spectra of Pep17 at: (a) pH 5.0 and (b) at pH 12.5. Reproduced from Reference [52] with permission from the Royal Society of Chemistry.

to set up a systematical reference for future FTIR studies of biological samples.

References

1. Rasola A, Neckers L, Picard D (2014) Mitochondrial oxidative phosphorylation TRAP(1)ped in tumor cells. Trends Cell Biol 24: 455-463.
2. Chaban Y, Boekema EJ, Dudkina NV (2014) Structures of mitochondrial oxidative phosphorylation supercomplexes and mechanisms for their stabilisation. Biochim Biophys Acta 1837: 418-426.
3. Dubnau D (1997) Binding and transport of transforming DNA by Bacillus subtilis: the role of type-IV pilin-like proteins--a review. Gene 192: 191-198.
4. McCauley MJ, Williams MC (2009) Optical tweezers experiments resolve distinct modes of DNA-protein binding. Biopolymers 91: 265-282.
5. Appert-Collin A, Baisamy L, Diviani D (2006) Regulation of g protein-coupled receptor signaling by a-kinase anchoring proteins. J Recept Signal Transduct Res 26: 631-646.
6. Mizejewski GJ (2011) Review of the putative cell-surface receptors for alpha-fetoprotein: identification of a candidate receptor protein family. Tumour Biol 32: 241-258.
7. Loredo-Trevino A, Gutierrez-Sanchez G, Rodriguez-Herrera R, Aguilar CN (2012) Microbial enzymes involved in polyurethane biodegradation: A review. J Polymers Envir 20: 258-265.
8. Srikanth K, Pereira E, Duarte AC, Ahmad I (2013) Glutathione and its dependent enzymes' modulatory responses to toxic metals and metalloids in fish--a review. Environ Sci Pollut Res Int 20: 2133-2149.
9. Lam RS, Nickerson MT (2013) Food proteins: a review on their emulsifying properties using a structure-function approach. Food Chem 141: 975-984.
10. Peters D, Peters J (1978) Structure and bonding in proteins: Electron organization in amide unit. J Mol Struct 50: 133-145.
11. Sachs JN, Engelman DM (2006) Introduction to the membrane protein reviews: the interplay of structure, dynamics, and environment in membrane protein function. Annu Rev Biochem 75: 707-712.
12. Adessi C, Soto C (2002) Beta-sheet breaker strategy for the treatment of Alzheimer's disease. Drug Development Res 56: 184-193.
13. Pauling L, Corey RB (1951) Configurations of Polypeptide Chains With Favored Orientations Around Single Bonds: Two New Pleated Sheets. Proc Natl Acad Sci USA 37: 729-740.
14. Wang C, Shah N, Thakur G, Zhou F, Leblanc RM (2010) Alpha-synuclein in alpha-helical conformation at air-water interface: implication of conformation and orientation changes during its accumulation/aggregation. Chem Commun (Camb) 46: 6702-6704.
15. Moran SD, Zanni MT (2014) How to Get Insight into Amyloid Structure and Formation from Infrared Spectroscopy. J Phys Chem Lett 5: 1984-1993.
16. Ganim Z, Chung HS, Smith AW, Deflores LP, Jones KC, et al. (2008) Amide I two-dimensional infrared spectroscopy of proteins. Acc Chem Res 41: 432-441.
17. Decatur SM (2006) Elucidation of residue-level structure and dynamics of polypeptides via isotope-edited infrared spectroscopy. Acc Chem Res 39: 169-175.
18. Decatur SM, Antonic J (1999) Isotope-edited infrared spectroscopy of helical peptides. J Am Chem Soc 121: 11914-11915.
19. Petty SA, Decatur SM (2005) Experimental evidence for the reorganization of beta-strands within aggregates of the Abeta(16-22) peptide. J Am Chem Soc 127: 13488-13489.
20. Barber-Armstrong W, Donaldson T, Wijesooriya H, Silva RA, Decatur SM (2004) Empirical relationships between isotope-edited IR spectra and helix geometry in model peptides. J Am Chem Soc 126: 2339-2345.
21. Susi H, Timasheff SN, Stevens L (1967) Infrared spectra and protein conformations in aqueous solutions. I. The amide I band in H2O and D2O solutions. J Biol Chem 242: 5460-5466.
22. Lappi SE, Smith B, Franzen S (2004) Infrared spectra of H(2)16O, H(2)18O and D(2)O in the liquid phase by single-pass attenuated total internal reflection spectroscopy. Spectrochim Acta A Mol Biomol Spectrosc 60: 2611-2619.
23. Ling S, Shao Z, Chen X (2014) Application of synchrotron FTIR imaging for cells. Progress in Chem 26: 178-192.
24. Wetzel DL, Slatkin DN, LeVine SM (1998) FT-IR microspectroscopic detection of metabolically deuterated compounds in the rat cerebellum: a novel approach for the study of brain metabolism. Cell Mol Biol (Noisy-le-grand) 44: 15-27.
25. Miller LM, Bourassa MW, Smith RJ (2013) FTIR spectroscopic imaging of protein aggregation in living cells. Biochim Biophys Acta 1828: 2339-2346.
26. Miller LM, Wang Q, Telivala TP, Smith RJ, Lanzirotti A, et al. (2006) Synchrotron-based infrared and X-ray imaging shows focalized accumulation of Cu and Zn co-localized with beta-amyloid deposits in Alzheimer's disease. J Struct Biol 155: 30-37.
27. Kurtikyan TS, Ford PC (2008) FTIR and optical spectroscopic studies of the reactions of heme models with nitric oxide and other NOx in porous layered solids. Coordin Chem Rev 252: 1486-1496.
28. Kobayashi M, Kobayashi M (1980) Effect of hydration on the amide I band in the binary solvents dioxane-D2O and dioxane-H2O. J Phys Chem 84: 781-785.
29. Bramanti E, Benedetti E, Nicolini C, Berzina T, Erokhin V, et al. (1997) Qualitative and quantitative analysis of the secondary structure of cytochrome C Langmuir-Blodgett films. Biopolymers 42: 227-237.
30. Chen X, Moser CC, Pilloud DL, Dutton PL (1998) Molecular orientation of Langmuir-Blodgett films of designed heme protein and lipoprotein maquettes. J Phys Chem B 102: 6425-6432.
31. Rajdev P, Chatterji D (2007) Thermodynamic and spectroscopic studies on the nickel arachidate-RNA polymerase Langmuir-Blodgett monolayer. Langmuir 23: 2037-2041.
32. Hasegawa T, Moriya D, Kakuda H, Li C, Orbulescu J, et al. (2005) Fibril-like aggregate formation of peptide carboxylate Langmuir films analyzed by surface pressure, surface dipole moment, and infrared spectroscopy. J Phys Chem B 109: 12856-12860.
33. Dluhy RA, Cornell DG (1985) In situ measurement of the infrared spectra of insoluble monolayers at the air-water interface. J Phys Chem 89: 3195-3197.
34. Dziri L, Desbat B, Leblanc RM (1999) Polarization modulated FT-IR spectroscopy studies of acetylcholinesterase secondary structure at the air-water interface. J Am Chem Soc 121: 9618-9625.
35. Wang C, Zheng J, Zhao L, Rastogi VK, Shah SS, et al. (2008) Infrared reflection-absorption spectroscopy and polarization-modulated Infrared Reflection-Absorption Spectroscopy studies of the organophosphorus acid anhydrolase Langmuir monolayer. J Phys Chem B 112: 5250-5256.
36. Wang C, Micic M, Ensor M, Daunert S, Leblanc RM (2008) Infrared reflection-absorption spectroscopy and polarization-modulated infrared reflection-absorption spectroscopy studies of the aequorin Langmuir monolayer. J Phys Chem B 112: 4146-4151.
37. Wang C, Li C, Ji X, Orbulescu J, Xu J, et al. (2006) Peptidolipid as binding site of acetylcholinesterase: molecular recognition of paraoxon in Langmuir films. Langmuir 22: 2200-2204.
38. Wang C, Zheng J, Oliveira ON, Leblanc RM (2007) Nature of the interaction between a peptidolipid Langmuir monolayer and paraoxon in the subphase. J Phys Chem C 111: 7826-7833.
39. Du X, Miao W, Liang Y (2005) IRRAS studies on chain orientation in the monolayers of amino acid amphiphiles at the air-water interface depending on metal complex and hydrogen bond formation with the headgroups. J Phys Chem B 109: 7428-7434.
40. Combs JD, Wang C (2015) α-Helix facilitates proteins to form Langmuir monolayer: Surface properties and orientation studies of aequorin and a-synuclein at the air-water interface: ACS Symposium Series.
41. Maltseva E, Kerth A, Blume A, Mohwald H, Brezesinski G (2005) Adsorption of amyloid beta (1-40) peptide at phospholipid monolayers. Chembiochem 6: 1817-1824.
42. Gaggelli E, Kozlowski H, Valensin D, Valensin G (2006) Copper homeostasis and neurodegenerative disorders (Alzheimer's, prion, and Parkinson's diseases and amyotrophic lateral sclerosis). Chem Rev 106: 1995-2044.
43. Varadarajan S, Yatin S, Aksenova M, Butterfield DA (2000) Review: Alzheimer's amyloid beta-peptide-associated free radical oxidative stress and neurotoxicity. J Struct Biol 130: 184-208.
44. Head JF, Inouye S, Teranishi K, Shimomura O (2000) The crystal structure of the photoprotein aequorin at 2.3 A resolution. Nature 405: 372-376.

45. Belbachir K, Lecomte S, Ta HP, Petibois C, Desbat B (2011) Orientation of molecular groups of fibers in nonoriented samples determined by polarized ATR-FTIR spectroscopy. Anal Bioanal Chem 401: 3263-3268.

46. Huo Q, Dziri L, Desbat B, Russell KC, Leblanc RM (1999) Polarization-modulated infrared reflection absorption spectroscopic studies of a hydrogen-bonding network at the air-water interface. J Phys Chem B 103: 2929-2934.

47. Smith BM, Franzen S (2002) Single-pass attenuated total reflection Fourier Transform Infrared Spectroscopy for the analysis of proteins in H2O solution. Anal Chem 74: 4076-4080.

48. Smith BM, Oswald L, Franzen S (2002) Single-pass attenuated total reflection Fourier Transform Infrared Spectroscopy for the prediction of protein secondary structure. Anal Chem 74: 3386-3391.

49. Hasegawa T (2015) Quantitative comparative techniques of Infrared spectra of a thin film: Acs Symposium Series.

50. Sarroukh R, Goormaghtigh E, Ruysschaert JM, Raussens V (2013) ATR-FTIR: a "rejuvenated" tool to investigate amyloid proteins. Biochim Biophys Acta 1828: 2328-2338.

51. Shai Y (2013) ATR-FTIR studies in pore forming and membrane induced fusion peptides. Biochim Biophys Acta 1828: 2306-2313.

52. Li S, Potana S, Keith DJ, Wang C, Leblanc RM (2014) Isotope-edited FTIR in H2O: determination of the conformation of specific residues in a model Î±-helix peptide by 13C labeled carbonyls. Chem Commun (Camb) 50: 3931-3933.

53. Miyazawa T (1960) Perturbation treatment of the characteristic vibrations of polypeptide chains in various configurations. J Chem Phys 32: 1647.

54. Miyazawa T, Blout ER (1961) The Infrared spectra of polypeptides in various conformations: Amide I and II bands. J Am Chem Soc 83: 712-719.

55. Susi H, Byler DM (1983) Protein structure by Fourier transform infrared spectroscopy: second derivative spectra. Biochem Biophys Res Commun 115: 391-397.